Applied Physics B (2018) 124:116
https://doi.org/10.1007/s00340-018-6986-x

Applied Physics B
Lasers and Optics

Surface plasmon resonance and nonlinear optical behavior of pulsed laser-deposited semitransparent nanostructured copper thin films

Rahul Kesarwani[1] · **Alika Khare**[1]

Received: 22 November 2017 / Accepted: 19 May 2018 / Published online: 29 May 2018
© Springer-Verlag GmbH Germany, part of Springer Nature 2018

Abstract
In this paper, surface plasmon resonance (SPR) and nonlinear optical properties of semitransparent nanostructured copper thin films fabricated on the glass substrate at 400 °C by pulsed laser deposition technique are reported. The thickness, linear absorption coefficient and linear refractive index of the films were measured by spectroscopic ellipsometer. The average particle size as measured via atomic force microscope was in the range of 12.84–26.02 nm for the deposition time ranging from 5 to 10 min, respectively. X-ray diffraction spectra revealed the formation of Cu (111) and Cu (200) planes. All these thin films exhibited broad SPR peak. The third-order optical nonlinearity of all the samples was investigated via modified z-scan technique using cw laser at a wavelength of 632.8 nm. The open aperture z-scan spectra of Cu thin film deposited for 5 min duration exhibited reverse saturation absorption whereas all the other samples displayed saturation absorption behavior. The nonlinear refractive index coefficient of these films showed a positive sign having the magnitude of the order of 10^{-4} cm/W. The real and imaginary parts of susceptibilities were also calculated from the z-scan data and found to be of the order of 10^{-6} esu.

1 Introduction

Surface plasmons (SPs) are the collective oscillations of the free electrons associated with metal at the metal–dielectric interface [1]. SPs are confined on the metallic surface with an exponentially decaying field in the neighboring media [2]. The resonant interaction between electrons near the surface of the metal and the electromagnetic field of the incident radiation results in a phenomena called SP resonance (SPR) [3]. SPR signal produced due to the interaction of metallic nanoparticles with the external electric field at the metal–dielectric interface has a typical response time of the order of picosecond [4]. Thus it can be utilized to fabricate fast plasmonics circuits [5], sensors [6], plasmonic chips [7], photonic devices [8], waveguides [9], etc. Bandwidth of SPR plays a significant role in deciding the specific application of metal nanoparticles. For example, larger bandwidth is favorable for plasmonic solar cells as it enhances the absorption efficiency [10], whereas narrow bandwidth is good for plasmonic sensing application [11]. Bandwidth is associated with the damping of collective oscillations. This damping can occur either through radiative (photon emission) or nonradiative processes (excitation of intraband or interband electronic transition/electron scattering process) [12]. Along with SPR, optical nonlinearity plays an important role in making fast photonic and electronic devices [13]. Metal nanoparticles embedded in dielectric have been studied extensively because of their large third-order nonlinearity [14] and fast response time (SPR signal) which leads to the applications in all optical switching devices [15]. The optical nonlinearity present in the metallic nanostructured thin films has been observed due to three types of mechanisms: (1) intraband transition, (2) interband transition, and (3) hot electron formation [16]. The SPR properties are strongly dependent on the type of metallic nanoparticle, size, shape, and surrounding medium [17, 18]. Optical nonlinear properties of metallic thin films depend on the average particle size of the nanoparticles on its surface [19]. The optical nonlinearity is manifested easily in terms of nonlinear absorption and nonlinear refractive index coefficient [20]. Nonlinear absorption can be of two types: reverse saturation absorption (RSA) and saturation absorption (SA). Metal films exhibiting SA can be of potential applications in passive mode locking in laser cavities, high power optical amplifiers, and optical limiters [21]. In the thin film, a large number of the

✉ Alika Khare
alika@iitg.ernet.in

[1] Laser and Photonic Lab, Department of Physics, IIT Guwahati, Guwahati, India

nano-sized atoms are arranged in a very closely packed manner. Subsequently, it interacts with nearby atoms resulting in splitting into new energy levels termed as the interband of aggregate system [22]. The interband transition can affect the optical properties of the semitransparent metallic thin film and thus, affects the plasmonic signal, linear and nonlinear optical (NLO) properties, and enhances the Raman signal [23–25]. Thin semitransparent plasmonic metallic films can be prepared by reactive magnetron sputtering [26], ion implantation [27], chemical vapor deposition [28], atomic layer deposition [29], and pulsed laser deposition (PLD) techniques [30, 31]. The PLD technique is very general and is applicable to any material including those having very high melting point. It is a single step process; free from any contamination as it does not required any additional chemicals in the entire process. Moreover, the size of the nanostructures can be controlled easily by deposition parameters, laser fluence, substrate to target distance, etc [32]. Among noble metals, Cu is an active material for such studies because it has low cost and high abundance relative to other noble metals [33]. Semitransparent film of Cu is suitable for the plasmonic devices as it possesses the large electrical conductivity as well as mechanical strength [34]. Apart from these properties, Cu nanoparticles exhibit SA behavior and large third-order NLO response [35]. In the present paper, the effect of film thickness and particle size of the semitransparent Cu thin films, fabricated via PLD, onto the SPR and NLO properties is presented. The Cu (111) phase in the PLD thin films was identified in X-ray diffractometer (XRD) spectra, and particle size distribution was obtained from atomic force microscope (AFM) images. The absorption spectra were recorded for detecting the SPR signal. The linear absorption coefficient, refractive index, and the thickness of the films were measured from spectroscopic ellipsometer. The z-scan experiment was performed for the measurement of NLO coefficients.

2 Experimental set-up

The nanostructured semitransparent Cu thin films were grown onto glass (coverslip) substrate inside a vacuum chamber via PLD technique. The PLD set-up used for deposition is shown in Fig. 1. The second harmonic of a Q-switched Nd:YAG laser (Quanta system Model No. HYL-01) was focused using a convex lens ($f = 35$ cm) onto a pure Cu target mounted on a motorized controlled-carrousel stage. The target was continuously rastered in a programmable manner to avoid its piercing during deposition and to maintain shot-to-shot reproducibility. The ablated material from the target is deposited onto the glass (coverslip) substrate placed 5 cm apart from the target and parallel to it. The films were deposited under vacuum, $\sim 10^{-6}$ mbar,

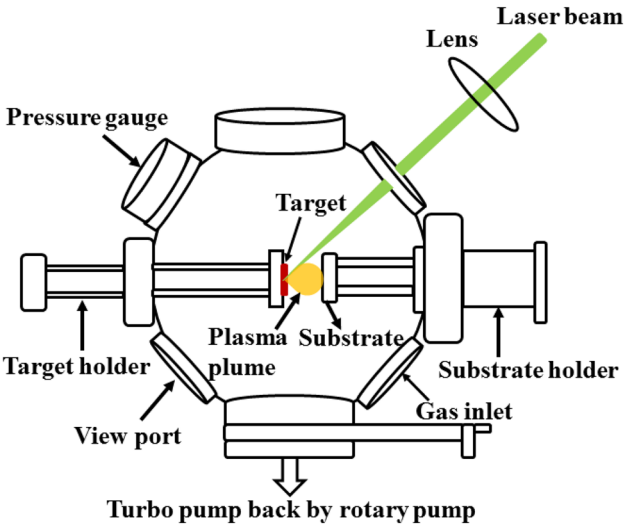

Fig. 1 Schematic of the pulsed laser deposition set-up

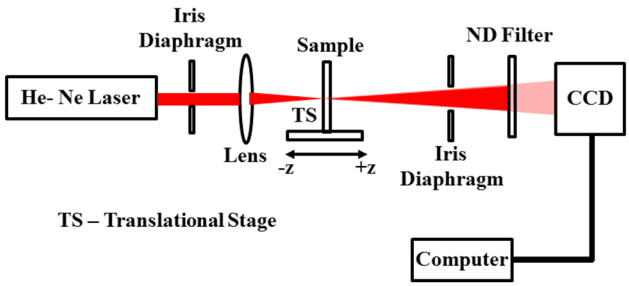

Fig. 2 Schematic of z-scan set-up

for a deposition time ranging from 5 to 10 min duration at a substrate temperature of 400 °C and the laser fluence of 4 J/cm^2. After the deposition, all the films were annealed at 400 °C under vacuum for a duration of 120 min. The crystallinity of these films was tested by XRD (Model No. Rigaku TTRAX III 18 kW) with Cu-K_α line. Thickness, linear absorption coefficient, and linear refractive index of the deposited metallic thin films were measured using spectroscopic Ellipsometer (Model No. SOPRA Semilab GES5-E).

The average particle size of the thin film was measured by AFM (Model No. Agilent 5500). SPR spectra of thin semitransparent metallic films were recorded via UV–vis–NIR spectrometer (Model No. Shimadzu UV 3101 PC). The nonlinear refractive index and absorption coefficient of films were measured using the modified z-scan technique [36]. This technique is based on the spatial beam broadening and narrowing of the Gaussian beam in far field because of optical nonlinearity present in the sample [20]. Figure 2 shows the experimental set-up for the modified z-scan measurement. A laser beam from a cw He–Ne laser (35 mW) was focused using a plano-convex lens ($f = 5$ cm) onto the Cu

film. The intensity of the laser beam at the focal point was estimated to be 1.46×10^3 W/cm^2. The transmitted beam through the sample was recorded as a function of sample position with respect to focus, on a charge-coupled device (CCD, Pixel fly), interfaced to a computer. An iris diaphragm of diameter 1.8 mm was placed in front of the laser to suppress the back-reflected light from the surface of the lens. Another iris diaphragm of 8 mm diameter was placed after the lens to avoid any unwanted scattered light entering into CCD. Neutral density filters were placed in front of CCD to prevent its saturation. In this set-up, information about the open as well as closed aperture (CA) z-scan can be deduced simultaneously from only one set of scanned images. The open aperture (OA) transmission, obtained by integrated intensity over the entire image as a function of distance with respect to focal point, gives the information about the absorptive nonlinearity present in the sample. The information about the CA z-scan is obtained by implementing a suitable synthetic aperture through a MATLAB programme in the central region of the images of OA z-scan and the integrated intensity of these partially masked images is the measure of the nonlinear refractive index coefficient [36].

3 Results and discussion

The thickness of the PLD-deposited films as a function of deposition time, measured using the ellipsometer, is listed in Table 1. It was observed to increase with the time. The minimum thickness was 27 nm for the deposition time of 5 min and that of 52 nm for 10 min duration. The XRD patterns of semitransparent Cu thin films deposited onto the glass substrate having thickness ranging from 27 to 52 nm are shown in Fig. 3. The films deposited for 5–7 min duration did not show any signature of XRD peak. This could be due to the reduction of the number of diffraction planes at such low film thickness. In the remaining thin samples, there was the clear signature of peaks at 43.30° and 50.70° corresponding to (111) and (200) reflection planes of Cu, respectively [37]. The AFM images (scan area 1 μm × 1 μm)

Table 1 Variation of the thin film thickness with deposition time

Deposition time (min)	Thickness (nm)
5	27
6	33
7	38
8	41
9	46
10	52

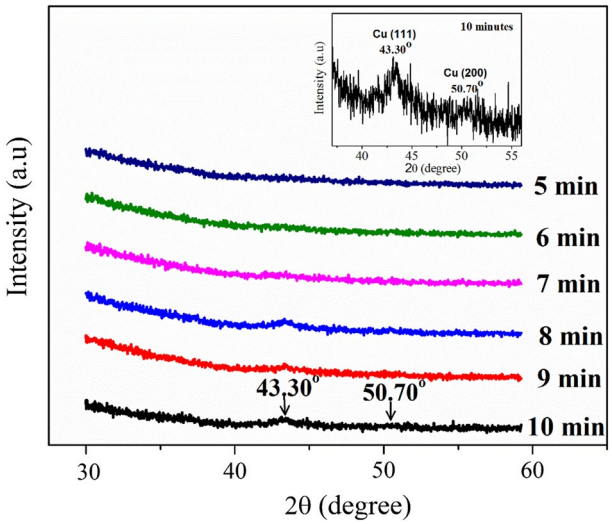

Fig. 3 XRD patterns of Cu thin films for different deposition time

of PLD-deposited Cu thin films shown in Fig. 4a–e display the uniform distribution of the nano-sized particles. It is observed that the shape of nanoparticles is conical as depicted in the 3D image of Fig. 4f for the film deposited at 10 min. The particle size distribution was estimated from 2D AFM images using Image J software. The estimated particle size is averaged over three different locations on the surface of the corresponding film. The inset in the AFM images of Fig. 4a–e gives the respective particle size distribution. The variation in the average particle size as a function of deposition time is shown in Fig. 5a, indicating the increase in the size from 12 to 26 nm for the deposition from 6 to 10 min, respectively.

The absorption spectra in the spectral range of 390–1400 nm of all the films are shown in Fig. 5b. It clearly exhibits the broad SPR peak in all these samples. In the present case, the SPR properties of the semitransparent nanostructured Cu thin films are presented in contrast to the suspended nanoparticles [38]. In the thin films, assembly of a large number of nanoparticles (closely packed), nearly conical in shape (Fig. 4), is accountable for a shift in the SPR peak position towards the longer wavelength side (near 800 nm) [39–41]. The peak position and bandwidth of SPR are obtained by fitting the absorption spectrum of Cu thin film with skew symmetric bi-Gaussian analytical equation [42]. The SPR peak position as a function of particle size is shown in Fig. 5c. It is observed that the SPR peak position initially decreases from 855 to 772 nm for the nanoparticle size of 12–16 nm and thereafter it exhibits a redshift from 778 to 833 nm for that of 23–26 nm, respectively. For the Cu nanoparticles of size above the 20 nm, the red shift in the SPR peak is in accordance with the classical electrodynamics theory [17]. This is attributed to the retardation effect as well as the contribution due to the multipolar

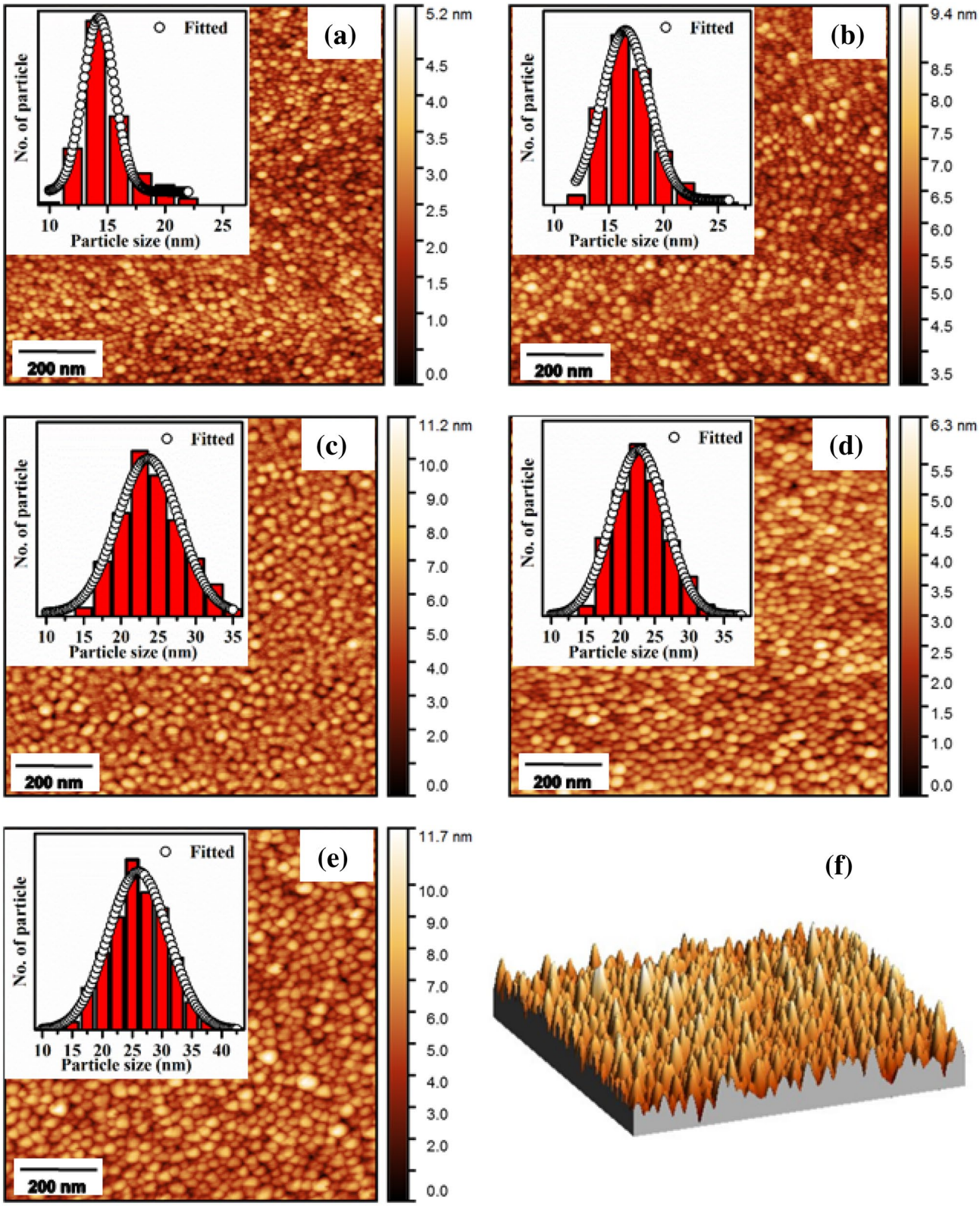

Fig. 4 AFM images of PLD Cu thin film deposited for **a** 6 min, **b** 7 min, **c** 8 min, **d** 9 min, **e** 10 min, and **f** 3D image of Cu thin film deposited for a duration of 10 min. The inset display the particle size distribution

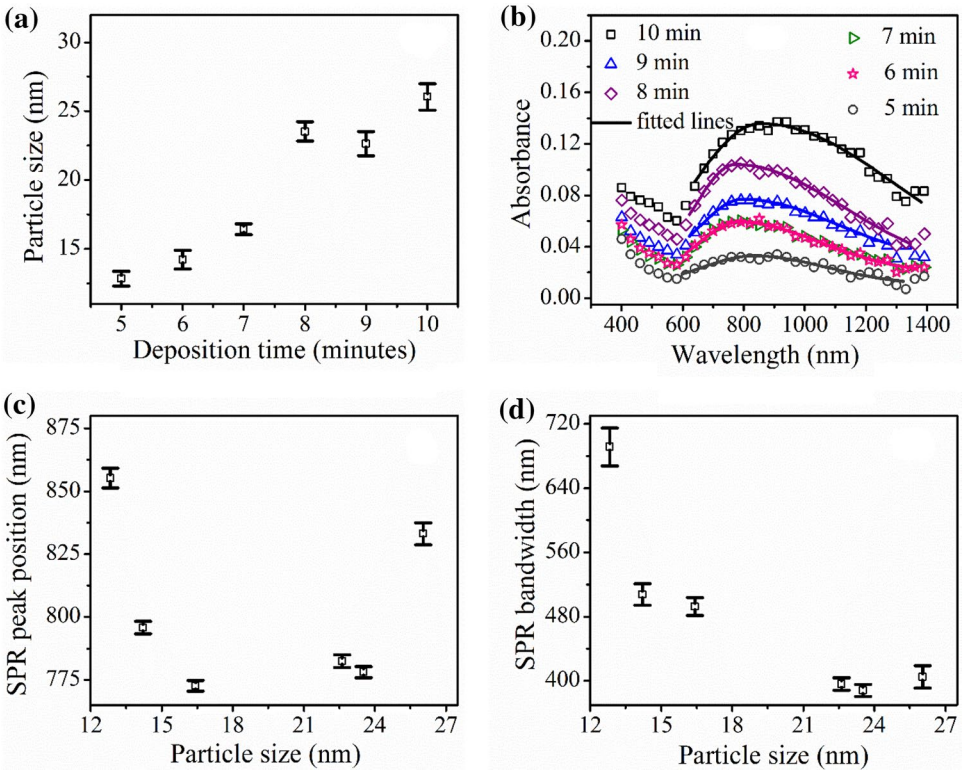

Fig. 5 **a** Variation of average particle size as a function of deposition time, **b** optical absorption spectra of semitransparent Cu thin films on glass substrate at various deposition time from 5 to 10 min, **c** variation of peak position, and **d** bandwidth of SPR with particle size

(quarter and octupole) terms [43]. Retardation is the effect of the phase difference between the field propagating from two different regions of the nanoparticles and it is dominant for coupling of large nanoparticle chains. For the nanoparticles of size below 20 nm, the discrepancy, the red shift rather than the blue shift with the decrease in the size has two possible reasons: (1) the scattering rate of conduction electron increases from the surface of the nanoparticles as the size of nanoparticles decreases and (2) surface damping constant of the SP increases as the size of the nanoparticles decreases resulting in decrease of the SPR frequency, i.e., the red shift of SPR with decreasing size [12, 18, 44]. The variation in the SPR bandwidth as a function of nanoparticles size is shown in Fig. 5d. In the present case, the bandwidth is broad and asymmetric in nature having a long tail toward the longer wavelength (Fig. 5b). Broadening and asymmetric nature of SPR could be attributed to the contribution of dipole modes compared with that of higher order modes along with the interband contribution of Cu nanoparticles [39]. In a deposited films, assembly of the nanoparticles is randomly distributed where each nanoparticle contributes to a characteristic absorption peak (through different order modes), depending on its size, shape, and environment. Hence, particles of various size and shape present in the assemblies result in broadening of SPR bandwidth. From Fig. 5d, it is observed that the bandwidth decreases from 690 to 385 nm with increasing particle's size from 12 to 23 nm, respectively. This inverse dependence of bandwidth on the size of the nanoparticles is due to the intrinsic size effect [40, 44]. With the further increase in particle size to 26 nm, the bandwidth increases slightly to 405 nm due to extrinsic size region having high enough concentration, where broadening varies in proportion with the size of the nanoparticles.

Figure 6a, b exhibit the OA and CA z-scan traces, respectively, for all the thin films. The nonlinear absorption coefficient (β), nonlinear refractive index coefficient (n_2) and real and imaginary part of NLO susceptibility ($\chi_R^{(3)}$, $\chi_I^{(3)}$) were estimated from the z-scan data using the following equations [45]:

$$T_{\text{open}}(z) = 1 \pm \frac{\beta I_o L_{\text{eff}}}{2^{3/2}[1 + (z/z_o)^2]} \tag{1}$$

$$T_{\text{closed}}(z) = 1 + \frac{4n_2 I_o L_{\text{eff}}(z/z_o)k}{[1 + (z/z_o)^2][9 + (z/z_o)^2]}, \tag{2}$$

$$\chi_R^3(\text{esu}) = 10^{-4}\frac{\epsilon_o n_o^2 c^2}{\pi} n_2 \left(\frac{\text{cm}^2}{\text{W}}\right), \tag{3}$$

$$\chi_I^3(\text{esu}) = 10^{-2}\frac{\epsilon_o n_o^2 c^2 \lambda}{4\pi^2}\beta(\text{cm/W}) \tag{4}$$

where T_{open} and T_{closed} are the normalized transmission for OA and CA z-scan, respectively. In the Eq. (1), the −ve sign

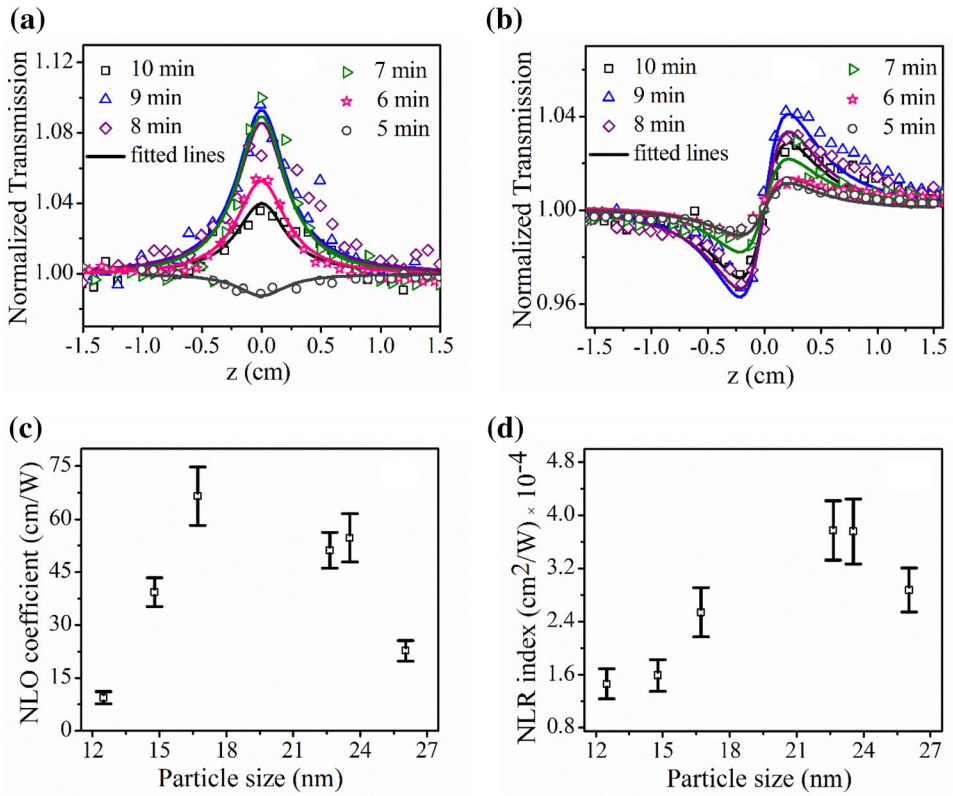

Fig. 6 Normalized transmittance *z*-scan spectra of Cu thin films **a** open and **b** closed spectrum. Variation with respect to particle size for **c** nonlinear absorption coefficient and **d** nonlinear refractive index coefficient

is RSA and +ve sign for SA. I_o, L_{eff}, z_o, k, ε_o, n_o, λ and c are the peak intensity at the focal plane, effective sample thickness, Rayleigh length, magnitude of wave vector, free-space permittivity, linear refractive index of thin film, wavelength of incident light and speed of light in vacuum, respectively. The parameters L_{eff} is defined as $L_{eff} = (1 - e^{-\alpha L})/\alpha$, where L is the actual sample thickness listed in Table 1 and α is the linear absorption coefficient. In the present experiment, the sample thickness is much less than the Rayleigh length, so thin sample approximation is well-satisfied. The linear refractive index 'n_o' and linear absorption coefficient 'α' are measured from the spectroscopic ellipsometric measurement and listed in Table 2 at a wavelength of $\lambda = 632.8$ nm.

The nonlinear absorption coefficient, nonlinear refractive index coefficient, real and imaginary parts of susceptibility of metallic films as a function of size of the Cu nanoparticles calculated for Eqs. (1)–(4). It has been reported in the literature that the origin of NLO properties in metallic thin films depends on several mechanisms [46]. One of the mechanisms responsible for nonlinear absorption in metals is due to the intraband transition of conduction electrons. This transition occurs due to the dipole oscillations of the free electrons [17]. The intraband transition decreases with the increase in the size of nanoparticles because as the size of the nanoparticle increases, the electric dipole contributions are less dominant compared to higher order pole. Another absorption mechanism is due to the interband contribution, where bound electrons are responsible for this transition between the d and s–p bands. Interband transition is independent of size and shape of the nanoparticles. There are some reports which show that the tuning of the size of the nanoparticles could affect the gap of electronic interband transition and hence, changes the absorption probability [47]. In the present work, the nonlinear absorption is attributed to the hot electron's contribution. In this mechanism, when the cw laser beam is

Table 2 List of linear and nonlinear optical constant of Cu thin metal film

Average particle size (nm)	Linear absorption (α cm^{-1})$\times 10^5$/ nature	n_o	Susceptibility (χ_R esu)$\times 10^{-6}$	Susceptibility (χ_I esu)$\times 10^{-6}$
12	1.56/Non-saturation	2.85	0.35	11.44
14	2.34/Saturation	2.48	0.28	35.49
16	2.20/Saturation	2.30	0.36	46.84
23	2.28/Saturation	2.35	0.60	44.17
23	2.17/Saturation	2.27	0.59	40.67
26	2.50/Saturation	2.38	0.48	19.20

incident upon a metal thin film, part of the total thermal energy that is produced by the laser-induced heating is absorbed in the metallic nanoparticles, where some part of the absorption energy promotes d-electrons in the vicinity of the X point of the first Brillouin zone to the conduction band, while the rest of the thermal energy is absorbed by the conduction electrons. When the thermal energy is provided to the metal nanoparticles, the redistribution of Fermi level due to heating effect occurs, leading to a modification of the dielectric constant, ε given by, $\epsilon = \epsilon_m + \delta\epsilon_m$, where $\delta\epsilon_m \cong \left(\partial\epsilon_m / \partial T\right)\delta T$ is the change in dielectric constant with temperature T, $\epsilon_m = \epsilon_{intraband} + \epsilon_{interband}$ and δT is the change in temperature of the free electrons [48–50]. This change in dielectric constant is responsible for controlling the values of nonlinear absorption and nonlinear refractive index coefficient. Figure 6c illustrates the variation of nonlinear absorption coefficient of Cu thin films with particle size. It is observed that the nonlinear absorption coefficient initially increases from 11.03 to 68.95 cm/W with the increase in size of nanoparticles from 12 to 16 nm, respectively, and thereafter it decreases with the further increase in particle size and goes down to 26.47 cm/W for the particle size of 26 nm. It could be due to the tuning of the gap of electronic intraband/interband transition [19]. The film deposited for 5 min duration having an average particle size of 12 nm exhibited RSA, whereas the rest of the samples display the SA behavior. This altered behavior of nonlinear absorption in this particular film could be due to two possible reasons: (i) modification in the interband/intraband transition level with size of the nanoparticles and (ii) smearing of the conduction band due to the hot electron's transition. Hot electron's effect loses its dominance with the increasing size of the nanoparticles [49]. The normalized CA z-scan curve as shown in Fig. 6b exhibits a pre-focal transmittance minimum (valley) followed by a post-focal transmittance maximum (peak). This valley–peak signature indicates the self-focusing property and results in positive nonlinear refractive index. The CA z-scan curves for all samples exhibit a peak–valley separation of $1.7z_o$, thus, confirming the presence of third-order nonlinearity. Figure 6d illustrates the variation of nonlinear refractive index coefficient with particle size. It is observed that, the nonlinear refractive index coefficient of Cu thin films increases from 1.71×10^{-4} to 4.54×10^{-4} cm^2/W with the size of the nanoparticles from 12 to 23 nm, but for larger sized nanoparticles of 26 nm, it decreases to 3.35×10^{-4} cm^2/W. The reason is due to the generation of the hot electrons through the thermal load and the number of electrons present on the surface of nanoparticles decrease with increase in its size for the larger particles.

Cu nanoparticles possess the large susceptibility compared to that of other noble metals because the contribution of the electronic transition from the top of the d band to the empty conduction band states is high [14]. The real and imaginary part of susceptibility obtained from Eqs. (3) and (4) are listed in Table 2 and it is observed to be of the order of 10^{-6} esu.

4 Conclusion

Cu nanostructured thin films were deposited via PLD technique at a substrate temperature of 400 °C. The deposited films were annealed at 400 °C near glass softening temperature (at 400 °C) to grow the nano-sized grain structure embedded in glass matrix to improve the plasmonic property. SPR peak position was observed to be blue-shifted with respect to the particle size initially and thereafter towards red for large-sized particles. The OA z-scan spectra of Cu film exhibited change from SA to RSA with the size of nanoparticles. This control on the NLO behavior is an important aspect for the photonics applications. The CA z-scan curves showed valley–peak signature indicating the self-focusing property and positive nonlinear refractive index.

Acknowledgements The Central Instrument Facility (CIF), IIT Guwahati is acknowledged for providing the Atomic Force Microscope and Spectroscopy Ellipsometer.

References

1. P.R. West, S. Ishii, G.V. Naik, N.K. Emani, V.M. Shalaev, A. Boltasseva, Laser Photonics Rev. **4**, 795–808 (2010)
2. J. Zhang, L. Zhang, W. Xu, J. Phys. D **45**, 113001 (2012)
3. H. Raether, *Surface Plasmons on Smooth Surfaces* (Springer, Berlin, 1988)
4. Y. Zhu, X. Hu, Y. Fu, H. Yang, Q. Gong, Sci. Rep. **3**, 2338 (2013)
5. E. Ozbay, Science **311**, 189–193 (2006)
6. V.M.N. Passaro, C.D. Tullio, B. Troia, M.L. Notte, G. Giannoccaro, F.D. Leonardis, Sensors **12**, 15558–15598 (2012)
7. C. Zhao, J. Zhang, Opt. Lett. **34**, 2417–2419 (2009)
8. R. Zia, J.A. Schuller, A. Chandran, M.L. Brongersma, Mater. Today **9**, 20–27 (2006)
9. S.A. Maier, H.A. Atwater, J. Appl. Phys. **98**, 011101 (2005)
10. K.R. Catchpole, A. Polman, Opt. Express **16**, 21793–21800 (2008)
11. J.N. Anker, W.P. Hall, O. Lyandres, N.C. Shah, J. Zhao, R.P. Van Duyne, Nat. Mater. **7**, 442–453 (2008)
12. S. Link, M.A. El-Sayed, J. Phys. Chem. B **103**, 4212–4217 (1999)
13. M. Kauranen, A.V. Zayats, Nat. Photonics **6**, 737–748 (2012)
14. T. Tokizaki, A. Nakamura, S. Kaneko, K. Uchida, S. Omi, H. Tanji, Y. Asahara, Appl. Phys. Lett. **65**, 941–943 (1994)
15. S. Dhara, C.-Y. Lu, P. Magudapathy, Y.-F. Huang, W.-S. Tu, K.-H. Chen, Appl. Phys. Lett. **106**, 023101 (2015)
16. B. Karthikeyan, M. Anija, C.S. Sandeep, T.M. Nadeer, R. Philip, Opt. Commun. **281**, 2933–2937 (2008)
17. C. Noguez, J. Phys. Chem. C **111**, 3806–3819 (2007)
18. O.A. Yeshchenko, I.M. Dmitruk, A.A. Alexeenko, A.V. Kotko, J. Verdal, A.O. Pinchuk, Plasmonics **7**, 685–694 (2012)

19. K. Wang, H. Long, M. Fu, G. Yang, P. Lu, Opt. Express **18**, 13874–13879 (2010)
20. M. Sheik-Bahae, A.A. Said, T.-H. Wei, D.J. Hagan, E.W. Van Stryland, IEEE J. Quantum Electron. **26**, 760–769 (1990)
21. S. Mohapatra, Y. Mishra, A. Warrier, R. Philip, S. Sahoo, A. Arora, D. Avasthi, Plasmonics **7**, 25–31 (2012)
22. J.P. Marton, B.D. Jordan, Phys. Rev. B **15**, 1719–1727 (1977)
23. G.C. Schatz, R.P.V. Duyne, in *Handbook of Vibrational Spectroscopy*, ed. by J.M. Chalmers, P.R. Griffiths (Wiley, Chichester, 2002)
24. K. Tanabe, J. Phys. Chem. C **112**, 15721–15728 (2008)
25. E. Cottancin, C. Langlois, J. Lerme, M. Broyer, M.-A. Lebeault, M. Pellarin, Phys. Chem. Chem. Phys. **16**, 5763–5773 (2014)
26. J. Su, Y. Liu, M. Jiang, X. Zhu, arXiv preprint arXiv:1412.2031 (2014)
27. Y.H. Wang, Y.M. Wang, J.D. Lu, L.L. Ji, R.G. Zang, R.W. Wang, Opt. Commun. **283**, 486–489 (2010)
28. R. Becker, A. Devi, J. Weiß, U. Weckenmann, M. Winter, C. Kiener, H.W. Becker, R.A. Fischer, Chem. Vap. Depos. **9**, 149–156 (2003)
29. Z. Li, A. Rahtu, R.G. Gordon, J. Electrochem. Soc. **153**, C787–C794 (2006)
30. A.T.T. Mostako, C.V.S. Rao, A. Khare, Rev. Sci. Instrum. **82**, 013101 (2011)
31. L.M. Kukreja, S. Verma, D.A. Pathrose, B.T. Rao, J. Phys. D **47**, 034015 (2013)
32. R. Eason, *Pulsed Laser Deposition of Thin Films: Applications-Led Growth of Functional Materials* (Wiley, 2007)
33. A. Bansal, S. Verma, Phys. Lett. A **379**, 163–169 (2015)
34. L. Lu, Y. Shen, X. Chen, L. Qian, K. Lu, Science **304**, 422–426 (2004)
35. R. Haglund, R. Magruder, K. Becker, R. Zuhr, J. Wittig, L. Yang, Opt. Lett. **18**, 373–375 (1993)
36. I. Kumar, A. Khare, Opt. Laser Technol. **77**, 51–54 (2016)
37. V. Figueiredo, E. Elangovan, G. Goncalves, P. Barquinha, L. Pereira, N. Franco, E. Alves, R. Martins, E. Fortunato, Appl. Surf. Sci. **254**, 3949–3954 (2008)
38. Q.-C. Sun, Y. Ding, S.M. Goodman, H.H. Funke, P. Nagpal, Nanoscale **6**, 12450–12457 (2014)
39. V.N. Rai, A.K. Srivastava, C. Mukherjee, S.K. Deb, Appl. Opt. **51**, 2606–2615 (2012)
40. U. Kreibig, M. Vollmer, *Optical Properties of Metal Clusters* (Springer, Berlin, 2013)
41. V. Truong, G. Scott, JOSA **67**, 502–510 (1977)
42. T. Buys, K. De Clerk, Anal. Chem. **44**, 1273–1275 (1972)
43. T.J. Davis, K.C. Vernon, D.E. Gómez, Opt. Express **17**, 23655–23663 (2009)
44. S. Link, M.A. El-Sayed, Int. Rev. Phys. Chem. **19**, 409–453 (2000)
45. G.P. Bharti, A. Khare, Opt. Mater. Express **6**, 2063–2080 (2016)
46. F. Hache, D. Ricard, C. Flytzanis, U. Kreibig, Appl. Phys. A **47**, 347–357 (1988)
47. B. Balamurugan, T. Maruyama, J. Appl. Phys. **102**, 034306 (2007)
48. G. Eesley, Phys. Rev. B **33**, 2144 (1986)
49. C. Voisin, D. Christofilos, N. Del Fatti, F. Vallée, B. Prével, E. Cottancin, J. Lermé, M. Pellarin, M. Broyer, Phys. Rev. Lett. **85**, 2200–2203 (2000)
50. R.D. Averitt, S.L. Westcott, N.J. Halas, J. Opt. Soc. Am. B **16**, 1814–1823 (1999)